Available online at www.sciencedirect.com

ScienceDirect

Nuclear Physics A 853 (2011) 1–25

NUCLEAR PHYSICS A

www.elsevier.com/locate/nuclphysa

Mass distribution in the bremsstrahlung-induced fission of ^{232}Th, ^{238}U and ^{240}Pu

H. Naik [a,*], V.T. Nimje [b], D. Raj [c], S.V. Suryanarayana [d], A. Goswami [a], Sarbjit Singh [a], S.N. Acharya [b], K.C. Mittal [b], S. Ganesan [c], P. Chandrachoodan [e], V.K. Manchanda [a], V. Venugopal [a], S. Banarjee [f]

[a] *Radiochemistry Division, Bhabha Atomic Research Centre, Mumbai, 400085, India*
[b] *Accelerator and Pulse Power Division, BARC, Mumbai, 400085, India*
[c] *Reactor Physics Design Division, BARC, Mumbai, 400085, India*
[d] *Nuclear Physics Division, BARC, Mumbai, 400085, India*
[e] *Board of Research in Nuclear Science, BARC, Mumbai, 400085, India*
[f] *Chairman, Atomic Energy Commission, Mumbai, 400085, India*

Received 30 April 2010; received in revised form 7 January 2011; accepted 11 January 2011

Available online 20 January 2011

Abstract

The yields of various fission products in the 10 MeV bremsstrahlung-induced fission of ^{232}Th, ^{238}U and ^{240}Pu were determined using a recoil catcher and off-line γ-ray spectrometric techniques. From the yield data, mass yield distributions were obtained using charge distribution corrections. The higher yields of fission products around mass numbers 133–135, 138–140, 143–145 and their complementary products in the neutron and bremsstrahlung-induced fission of ^{232}Th, ^{238}U and ^{240}Pu were interpreted based on nuclear structure effects. From the mass yield distribution, the peak-to-valley (P/V) ratio was also obtained for the above fissioning systems. The present data, along with data from the literature on different bremsstrahlung- and mono-energetic neutron-induced fissions of ^{232}Th and ^{238}U are interpreted to examine the influence of excitation energy on the peak to valley ratio. For the same compound nucleus ^{240}Pu*, the data in the 10–30 MeV bremsstrahlung-induced fission of ^{240}Pu were compared with similar data of thermal to 14 MeV neutron-induced fission of ^{239}Pu and the spontaneous fission of ^{240}Pu to examine the role of excitation energy due to bremsstrahlung radiation and mono-energetic neutrons.

* Corresponding author.
E-mail address: naikhbarc@yahoo.com (H. Naik).

0375-9474/$ – see front matter
doi:10.1016/j.nuclphysa.2011.01.009

Keywords: NUCLEAR REACTIONS $^{+232}$Th, $^{+238}$U, $^{+240}$Pu(γ, F); $E = 10$ MeV bremsstrahlung; measured fission yields and mass distributions via off-line γ-spectroscopy using an HPGe detector. Comparison with neutron-induced fission data

1. Introduction

Recently, significant effort has been aimed at generating nuclear power based on the concept of fast rector [1,2] and advanced heavy water reactor (AHWR) [3] to fulfill the increased demand for power production. However, most of the present reactors operating in the world are light water reactors (PWR & BWR) or heavy water reactors (HWR), which are based on enriched or natural uranium as fuel. These reactors produce long-lived minor actinides and fission products, which are radiotoxic and hazardous to human life. The problem of radiotoxic long-lived minor actinides and fission products can be solved by using an accelerator-driven sub-critical system (ADS) [4,5]. The main purpose of an ADS is the transmutation of long-lived fission products and incineration of long-lived minor actinides. This may solve the problem of radioactive waste while generating of energy for electricity production. In ADS high energy (GeV) protons from an accelerator strike a heavy element target like W, Pb, Bi, Th and U yielding a large number of neutrons by spallation reactions. The spallation target becomes a source of neutrons, which drives the fission chain in a sub-critical core. In the spallation processes, along with high-energy neutrons, high-energy photons are also produced, which can cause fission of the spallation target and long-lived minor actinides in the sub-critical core. Thus, it is also important to measure the yields of the fission products in the photon- and fast neutron-induced fission of actinides. This is because the yields of fission products are needed for decay heat calculations [6], which are necessary for the design of ADS. Additionally, the yields of fission products are also needed for mass and charge distribution studies, which can provide valuable information for understanding the process of nuclear fission.

Studies of the mass and charge distribution in the low energy fission of actinides provide important information about the nuclear structure effect and dynamics of descent from saddle to scission [7–9]. The yields of fission products relevant to mass and charge distribution studies in the neutron-induced fission of actinides from Ac to Fm and the spontaneous fission of heavier actinides are available in different compilations [10–13]. However, most of the fission yield data available in the literature are for the thermal neutron- [10–13] or reactor neutron-induced [14–22] fission of actinides. For mono-energetic neutron-induced fission, most of the data available are for actinides induced by either 3 or 14 MeV neutrons [23–37]. Some of the data on various mono-energetic neutron-induced fissions of actinides are available for specific nuclides such as ^{232}Th [38–42], ^{233,235,238}U [43–48], ^{237}Np [49,50] and ^{239}Pu [33,51]. Similarly yields of fission fragments in the excitation energy range of the GDR region due to electromagnetic fission in inverse kinematics [52–54] are available for neutron-deficient lighter actinides such as $^{214–223}$Ac, $^{220–229}$Th, $^{224–232}$Pa and $^{231–234}$U. On the other hand, yields of fission products in the bremsstrahlung-induced fission of actinides are available in a broad energy range for a limited number of actinides including ^{232}Th [55–60], ^{235,238}U [61–74] and ^{240,242,244}Pu [75–78]. Most of the yield data on fission products available in the 9 MeV to several GeV bremsstrahlung-induced fission of ^{232}Th [55–59] and ^{235,238}U [61–67] are based on radiochemical separation and beta counting or γ-ray spectrometric techniques. In the recent past, some data on the mass distribution of ^{232}Th [60], ^{235}U [74] and ^{238}U [73] have become available for bremsstrahlung energies at near barrier using off-line γ-ray spectrometric techniques. Some data on the bremsstrahlung-induced fission of ^{235,238}U in the energy range of 12–70 MeV were obtained using off-line γ-ray spectrometric techniques [68–70] and physical measurements [71,72]. On the other hand, the yield data on the fission products in the 12–30 MeV bremsstrahlung-induced fission of ^{240,242,244}Pu [75–77] are from physical measurements. This is because only a limited amount of even–even Pu-isotopes are available due to their high alpha activity. Some of the yield data of fission products in the 18.1 and 20.7 MeV bremsstrahlung-induced fission of ^{242}Pu became available in the recent past [78] based on off-line γ-ray spectrometric techniques. The yields of fission products are not available in the bremsstrahlung-induced fission of Pu-isotopes at lower or higher energies based on either physical or off-line γ-ray spectrometric techniques. The yield data of fission products at lower energies are very much important for the study of nuclear structure effects such as shell closure proximity and the even–odd effect.

Based on the above data, it can be seen that in the neutron- [14–51] and bremsstrahlung-induced [55–78] fission of actinides, the yields of fission products are higher around mass numbers 133–135, 138–140 and 143–145 and their complementary products depending on the mass of the fissioning systems [21,22]. However, the yield of fission products around mass numbers 133–135 is more pronounced compared to mass numbers 143–145, in both neutron- [28–33] and bremsstrahlung-induced [61–74] fission of uranium isotopes and heavier actinides. In the electromagnetic fission of lighter actinides [52–54], higher yields of fission products around mass numbers 133–135 corresponding to a most probable charge of 52 have been observed. Similarly, higher yields of fission products around mass numbers 133–135 in the 3 and 14 MeV mono-energetic neutron-induced [28–34] and in the 9, 15 and 31 MeV bremsstrahlung-induced [59] fission of ^{232}Th have also been observed earlier. However, in the 6.44–13.13 MeV bremsstrahlung-induced fission of ^{232}Th [60], yields of fission products are more pronounced around mass numbers 143–145 compared to mass numbers 133–135, which is contradictory to the earlier observations [23–27,59]. Besides this, it can be found in Ref. [60] that a third peak for the symmetric products was observed in the 6.44–13.13 MeV bremsstrahlung-induced fission of ^{232}Th. This is not clear from the radiochemical data on the 9 and 10 MeV bremsstrahlung-induced fission of ^{232}Th [59] due to a lack of sufficient data around the symmetric region. The observation of a third peak of symmetric products in the bremsstrahlung- and neutron-induced fission of ^{232}Th is interesting in view of probing the potential energy surface. In view of the above observations, in the present work, we have determined the yields of fission products in the 10 MeV bremsstrahlung-induced fission of ^{232}Th, ^{238}U and ^{240}Pu using a recoil catcher and off-line γ-ray spectrometric techniques. A bremsstrahlung energy of 10 MeV was chosen based on the average excitation energy of the fissioning nucleus, which is comparable to the excitation energy in the case of reactor neutron (average $E_n = 1.9$ MeV)-induced fission of ^{232}Th [14–16], ^{238}U [21,22] and ^{240}Pu [18,22]. These data, along with similar data in the bremsstrahlung- and neutron-induced fission of ^{232}Th, ^{238}U and ^{240}Pu over a wide range of energy are interpreted from the point of view of nuclear structure effects and excitation energy transfer. For the compound nucleus ^{240}Pu*, the experimental data in the bremsstrahlung-induced fission of ^{240}Pu were compared with similar data of thermal [11–13] and mono-energetic neutron-induced [33,51] fission of ^{239}Pu and spontaneous fission of ^{240}Pu [75,79]. This comparison can provide information about different fission mechanisms of the bremsstrahlung- and mono-energetic neutron-induced fission of actinides due to incomplete/non-compound energy mixing in the former case. The dependence of the nuclear structure effect (e.g., shell closure proximity and even–odd effect) on the excitation energy in neutron- and bremsstrahlung-induced fission was also examined.

2. Experimental methods

In the present experiment, we measured fission product yields with a bremsstrahlung spectrum having an endpoint energy of 10 MeV. The experiment was carried out using the 10 MeV electron LINAC of the electron beam centre (EBC) at Kharghar, Navi-Mumbai, India. The endpoint bremsstrahlung was produced by a 10 MeV electron beam impinging on a 1 mm thick tantalum metal foil placed at distance of 10 cm on a suitable stand facing the electron beam aperture.

2.1. Target preparation and irradiation

In the case of ^{232}Th and ^{238}U, metal target foils were wrapped with 0.025 mm thick super pure aluminum foil. The amount of ^{232}Th was 0.2822 gm with an area of 2.72 cm^2, whereas in the case of ^{238}U the amount was 0.2414 gm with an area of 2.5 cm^2. The aluminum wrapper captures the fission products recoiling out from the fission of Th and U metal foil during irradiation. In the case of the ^{240}Pu target, an amount of 90 µg of plutonium in the form of a nitrate solution was dried on a 0.025 mm thick aluminum foil and folded into a small square having an area 1.0 cm^2. Additionally, the target was wrapped with one more layer of aluminum foil of the same thickness to prevent any loose alpha contamination [22].

Each of the target ^{232}Th, ^{238}U and ^{240}Pu samples was placed below the tantalum foil for individual irradiation. Each target assembly was then irradiated for 4 to 5 h with the bremsstrahlung produced by bombarding the tantalum metal foil with a 10 MeV electron beam. The current of the electron beam during irradiation was 50 mA with a frequency of 400 Hz and a pulse width of 10 µs. The irradiated target assembly was cooled for 0.5–1.5 h. Then, the target with an aluminum catcher was mounted on a Perspex plate and taken for γ-ray counting.

2.2. γ-ray spectrometric analysis

The γ-ray activities of the fission products in the samples at a fixed geometry were measured [21,22] by using an energy- and efficiency-calibrated 80 c.c. HPGe detector coupled to a PC-based 4096 channel analyzer. The resolution of the detector system was 2.0 keV at 1332.0 keV of ^{60}Co. The dead time of the detector system during counting was always kept at less than 10% by placing the sample a suitable distance from the detector to avoid the pile-up effect. The γ-ray counting of the sample was done in live time mode and was followed as a function of time. In the case of ^{240}Pu, the γ-ray counting of the fission products was done by placing the irradiated sample quite close to the detector. On the other hand, in the case of ^{232}Th and ^{238}U, the γ-ray counting of the fission products was done by placing the irradiated sample further from the detector. This was because the amount used for irradiation of ^{240}Pu was significantly less than that used for ^{232}Th and ^{238}U.

3. Calculations and results

3.1. Calculation of excitation energy

In the present experiment, we measured yields of fission products with a bremsstrahlung having an endpoint energy of 10 MeV. In such cases, the average excitation energy ($E^*(E_e)$) of the fissioning nuclei can be obtained by using the following relation [68],

$$E^*(E_e) = \frac{{}_0\int^{E_e} E N(E_e, E)\sigma_F(E)\,dE}{{}_0\int^{E_e} N(E_e, E)\sigma_F(E)\,dE} \tag{1}$$

where $N(E_e, E)$ is the number of photons at energy E for electron energy E_e and $\sigma_F(E)$ is the fission cross-section as a function of the photon energy (E).

The bremsstrahlung spectrum $N(E_e, E)$ corresponding to an incident electron energy (E_e) was calculated using EGS4 computer code [80], as is usually done [68–74]. The photo-fission cross-sections of ^{232}Th and ^{238}U in the sub-barrier region [81] and energy range of 5–18.3 MeV [82,83] are available. Similarly, the photo-fission cross-section of ^{240}Pu in the sub-barrier region [84] and energy range of 10–30 MeV [75] is also available. The available data on the photo-fission cross-sections of ^{232}Th and ^{238}U are inconsistent [83,84]. The photo-fission cross-sections of the targets ^{232}Th*, ^{238}U* and ^{240}Pu* as a function of photon energy were calculated using TALYS code [85].

TALYS [85] can be used for the calculation of nuclear reactions and fission cross-sections that involve targets of 12 and heavier mass units and projectiles like photons, neutrons, protons, ^{2}H, ^{3}H, ^{3}He and alpha particles in the energy range of 1 keV to 200 MeV. In TALYS, several options are included for the choice of fission barrier parameters. In the present work, we calculated photon-induced fission cross-section ($\sigma_F(E)$) of ^{232}Th, ^{238}U and ^{240}Pu targets using the default option of the fission parameters in the TALYS code [85]; by ignoring the symmetric scission mode. The default parameters in the TALYS code define the asymmetric fission barrier. The inner and outer fission barrier values used in the present calculation were 5.8 and 6.7 MeV for ^{232}Th, 6.3 and 5.5 MeV for ^{238}U and 6.05 and 5.15 MeV for ^{240}Pu. The transmission coefficients through fission barriers were calculated with the Hill–Wheeler formula. All possible outgoing channels for a given γ-ray energy were considered. However, the cross-section for the photo-fission was especially looked for and collected. The partial-wave cross-sections for the $J^\pi K = 1^-0$, 1^-1 and 2^+0 photo-fission channels were taken care of to determine the total photo-fission cross-section. In the case of ^{232}Th, the damping of the vibrational states in the second and third well was not considered. The photon-induced fission cross-sections obtained from the TALYS calculations are plotted in Fig. 1. The values obtained from the TALYS calculations showed a similar structure, with slight differences in magnitude compared to the experimental values [75, 81–84]. The slight difference in magnitude was probably due to the use of the default parameters for fission barriers in the TALYS calculation.

In Eq. (1), the value of $N(E_e, E)$ from the EGS4 code [80] and $\sigma_F(E)$ from the TALYS code [85] were used to calculate the average excitation energy, as reported by us in the bremsstrahlung-induced fission of ^{209}Bi [86]. For the 10 MeV bremsstrahlung energy, the average excitation energies were found to be 7.35, 7.55 and 7.61 MeV for the fissioning systems ^{232}Th*, ^{238}U* and ^{240}Pu*, respectively. The excitation energies for the fissioning systems ^{232}Th* and ^{238}U* obtained after using theoretical fission cross-sections from the TALYS were found to be in good agreement with the data [60,73] where experimental fission cross-sections were used. This may be due to the fact that the average excitation energy obtained from Eq. (1) is more sensitive to the shape of the fission excitation function, but less sensitive to the magnitude of the fission cross-section at lower energy.

3.2. Calculation of yields of fission products from the photo-peak areas

The photo-peak areas of different γ-rays of nuclides of interest were calculated by subtracting the linear Compton background from their net peak areas. From the number of γ-rays detected

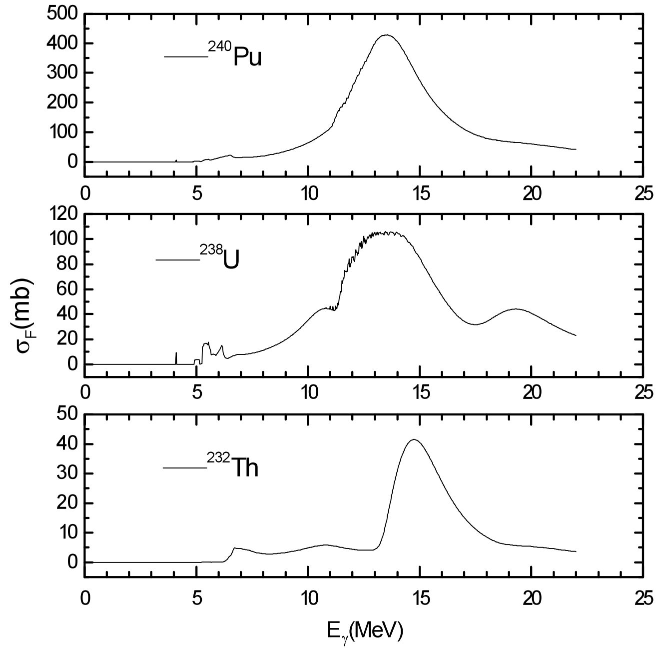

Fig. 1. Plot of theoretically calculated photo fission cross-section of ^{232}Th, ^{238}U and ^{240}Pu as a function of photon energy using the TALYS 1.2 computer code.

(N_{obs}) under the photo peak of each individual fission product, their cumulative yields (Y_R) relative to ^{135}I were calculated by using the standard decay equation [21,86]

$$N_{\text{obs}}(CL/LT) = n\sigma_F(E)\Phi I_\gamma \varepsilon Y_R\left(1-e^{-\lambda t}\right)e^{-\lambda T}\left(1-e^{-\lambda CL}\right)/\lambda, \tag{2}$$

where 'n' is the number of target atoms and $\sigma_F(E)$ is the photo-fission cross-section of the target nuclei in the bremsstrahlung spectrum with an endpoint energy of 10 MeV. Here, $\Phi = {}_{E_b}\int^{E_e} \phi\, dE$ is the bremsstrahlung flux with photon flux ϕ from the fission barrier (E_b) to the endpoint energy (E_e), 'ε' and I_γ are the efficiency and branching intensity for the γ-ray of the fission product nuclide of interest, t and T are the irradiation and cooling times, and CL and LT are the clock time and live time of counting, respectively.

The nuclear spectroscopic data, such as the γ-ray energy, branching intensity and half-life of the fission products were taken from Refs. [87,88]. The cumulative yields (Y_R) of the fission products relative to fission rate monitor ^{135}I were calculated using Eq. (2). From the relative cumulative yields (Y_R) of the fission products, their relative mass chain yields (Y_A) were calculated by using Wahl's prescription of charge distribution [13]. According to this, the fractional cumulative yield (FCY) of a fission product in an isobaric mass chain is given as

$$FCY = \frac{EOF^{a(Z)}}{\sqrt{2\pi\sigma_Z^2}} {}_{-\infty}\int^{Z+0.5} \exp\left[-(Z-Z_P)^2/2\sigma_Z^2\right] dZ, \tag{3}$$

$$Y_A = Y_R/FCY, \tag{4}$$

where Z_P is the most probable charge and σ_Z is the width parameter of an isobaric yield distribution. $EOF^{a(Z)}$ is the even–odd effect with $a(Z) = +1$ for even Z nuclides and -1 for odd Z nuclides.

It is evident from the above equation that in an isobaric mass chain, it is necessary to have knowledge of Z_P, σ_Z and $EOF^{a(Z)}$ to calculate the FCY value of a fission product and mass chain yield. In the bremsstrahlung-induced fission of ^{232}Th and ^{238}U, the Z_P, σ_Z and $EOF^{a(Z)}$ values can be obtained from the fission yield data of Refs. [89,90]. However, there is no fission yield data in the literature for the 10 MeV bremsstrahlung-induced fission of ^{240}Pu to obtain the values of Z_P, σ_Z and $EOF^{a(Z)}$. On the other hand, there are systematic data on the charge distribution in the reactor neutron (average $E_n = 1.9$ MeV)-induced fission of ^{232}Th, ^{238}U and ^{240}Pu [91]. It can be seen in Refs. [89–91] that the average width parameter ($\langle\sigma_Z\rangle$) in the 10 MeV bremsstrahlung- and reactor neutron-induced fission of ^{232}Th and ^{238}U are nearly the same in spite of the small difference in N/Z values of the fissioning systems. Additionally, the average excitation energy in the 10 MeV bremsstrahlung- and reactor neutron-induced fission of ^{232}Th, ^{238}U and ^{240}Pu are also comparable. In view of this, the average width parameter ($\langle\sigma_Z\rangle$) values of 0.52 ± 0.08, 0.55 ± 0.07 and 0.57 ± 0.07 from Ref. [91] were used in the 10 MeV bremsstrahlung-induced fission of ^{232}Th, ^{238}U and ^{240}Pu, respectively. The mass dependence of the even–odd factor on σ_Z was not considered, which may give rise to an error of 3–5% in the FCY value.

The Z_P value of individual mass chain (A) for the above fissioning systems was calculated using the relation [13,92]

$$Z_P = Z_{UCD} \pm \Delta Z_P, \qquad Z_{UCD} = (Z_F/A_F)(A + \nu_A) \tag{5}$$

where Z_F and A_F are charge and mass of the fissioning system. Z_{UCD} is the most probable charge based on the unchanged charge density distribution, as suggested by Sugarman and Turkevich [92]. The $+$ and $-$ signs are applicable to light and heavy fragments, respectively. The symbol 'ν_A' is the number of neutrons emitted by the corresponding fragment and is evaluated according to the method of Erten and Aras [93]. Accordingly, ν_A for light (ν_L) and heavy (ν_H) fission product mass is given as

$$\nu_L = 0.531\nu + 0.062(A_L + 143 - A_F), \tag{6a}$$

$$\nu_H = 0.531\nu + 0.062(A_H - 143). \tag{6b}$$

ΔZ_P is the charge polarization given by Coryell et al. [94] as

$$\Delta Z_P = 0.5(Z_F - 92) + 0.19(A_F - 236) + 0.19(\nu - 2.45), \tag{7}$$

where ν is the average neutron number in the 10 MeV bremsstrahlung-induced fission of ^{232}Th, ^{238}U and ^{240}Pu. The ν value in the 10 MeV bremsstrahlung-induced fission of ^{232}Th and ^{238}U was taken as 2.17 [89] and 2.7 [90]. However, there are no data on the ν value in the 10 MeV bremsstrahlung-induced fission of ^{240}Pu. In view of that, a ν value of 3.0 was used based on its value in the 1.0 MeV neutron-induced fission of ^{239}Pu [51], which has a comparable excitation energy. This is justified because for the compound nucleus ^{240}Pu*, the excitation energy for 1.0 MeV neutron-induced fission of ^{239}Pu is 7.53 MeV with an average ν value of 3.01 [51]. In the thermal neutron-induced fission of ^{239}Pu, the excitation energy is 6.53 MeV with an average ν value of 2.9 [51]. Thus, within the excitation energy range of 6.53 to 7.53 MeV, the average ν value will vary from 2.9 to 3.01. In the 10 MeV bremsstrahlung-induced fission of ^{240}Pu the average excitation energy is 7.61 MeV, where a ν value of 3.0 can be safely adopted. This assumption of a ν value of 3.0 is also validated by its close agreement with the corresponding value in the reactor neutron-induced fission of ^{240}Pu [91], which has a comparable excitation energy.

The relative mass chain yields of the fission products obtained as mentioned above were normalized to a total yield of 200% to obtain the absolute mass chain yields. The absolute cumulative yield of the fission products in the 10 MeV bremsstrahlung-induced fission of ^{232}Th, ^{238}U and ^{240}Pu was obtained using the mass yield data and *FCY* values from Eq. (3). The cumulative yields of the fission products in the 10 MeV bremsstrahlung-induced fission of ^{232}Th, ^{238}U and ^{240}Pu along with the nuclear spectroscopic data from Refs. [87,88] are given in Tables 1–3, respectively. The absolute mass chain yields in the above fissioning systems from the present work are also given in the last column of Tables 1–3 for the respective fissioning systems. The uncertainty shown in the measured cumulative yield of individual fission products in Tables 1–3 is the statistical fluctuation of the mean value from two determinations. The overall uncertainty represents contributions from both random and systematic errors. The random error in the observed activity is due to counting statistics and is estimated to be 10–15%, which can be determined by accumulating the data for the optimum period of time, depending on the half-life of the nuclide of interest. Conversely, the systematic errors are due to the uncertainties in irradiation time (2%), detector efficiency calibration ($\sim 3\%$), half-life of nuclides of the fission products ($\sim 1\%$) and the γ-ray abundance ($\sim 2\%$), which are the largest variation in the literature [87,88]. Thus, the overall systematic error is about 4%. An upper limit of error of 11–16% was determined at for the fission product yields based on 10–15% random error and a 4% systematic error.

4. Discussion

The yields of fission products shown in Table 3 in the 10 MeV bremsstrahlung-induced fission of ^{240}Pu from the present work were determined for the first time. On the other hand, the yields of fission products in the 10 MeV bremsstrahlung-induced fission of ^{232}Th and ^{238}U from the present work shown in Tables 1 and 2, are in good agreement with the data from the literature [60,73]. The mass chain yield data in the 10 MeV bremsstrahlung-induced fission of ^{232}Th, ^{238}U and ^{240}Pu from Tables 1–3 are plotted in Figs. 2–5. The mass yield data of ^{232}Th plotted in Fig. 2 is in log scale, while they are in linear scale in Fig. 3. This was done to visualize the third peak in the valley region and fine structure in the high yield region, which is discussed below. The mass chain yield data in the reactor neutron-induced fission of ^{232}Th, ^{238}U and ^{240}Pu from Refs. [14, 21,22] are also plotted in Figs. 2–5 for comparison. Since the cumulative yield data are given in the neutron-induced fission of ^{232}Th [14,15], their mass chain yields were obtained by using a similar procedure [21] as mentioned above. The fission yield data of the reactor neutron (average $E_n = 1.9$ MeV)-induced fission were chosen instead of the yield data from the mono-energetic neutron-induced fission to examine the role of average excitation energy in reactor neutron- and bremsstrahlung-induced fission. The role of excitation energy due to the mono-energetic photon (neutron) compared to the bremsstrahlung (neutron) spectrum is discussed below.

It can be seen from Fig. 2 that in the mass yield distribution of 10 MeV bremsstrahlung- and reactor neutron-induced fission of ^{232}Th, there is a well-known third peak around the symmetric mass region. This is due to the different types of potential barrier for ^{232}Th compared to ^{238}U, as shown by Moller [95], who calculated the saddle point configurations against the mass asymmetric deformation. This has been proved by Schmidt et al. [52] and others [53,54] by carrying out the electromagnetic-induced fission of neutron-deficient lighter actinides from a relativistic radioactive ion beam. It has been shown by them [52–54] that the charge and mass yield distribution of neutron-deficient isotopes of Th (i.e. $^{226-229}$Th) is triple humped. Among

Table 1
Nuclear spectroscopic data and yields of fission products in the 10 MeV bremsstrahlung-induced fission of ^{232}Th.

Nuclide	Half-life	γ-ray Energy (keV)	γ-ray Abundance (%)	Cu.Y. (%)	M.Y. (%)
^{77}Ge	11.3 h	416.3	21.8	0.514 ± 0.135	0.519 ± 0.136
^{85}Kr^{m}	4.48 h	151.2	75.0	6.137 ± 0.406	6.162 ± 0.408
		304.9	14.0	6.178 ± 0.722	6.203 ± 0.725
^{87}Kr	76.3 m	402.6	49.6	6.545 ± 0.465	6.611 ± 0.470
^{88}Kr	2.84 h	196.3	25.9	5.787 ± 0.334	5.787 ± 0.334
^{91}Sr	9.63 h	749.8	23.6	5.903 ± 0.124	5.903 ± 0.124
		1024.3	33.0	6.813 ± 0.395	6.813 ± 0.395
^{92}Sr	2.71 h	1384.9	90.0	5.278 ± 0.167	5.326 ± 0.169
^{95}Zr	64.02 d	756.7	54.0	5.758 ± 0.886	5.758 ± 0.886
^{97}Zr	16.91 h	743.4	93.0	2.257 ± 0.152	2.278 ± 0.152
^{99}Mo	65.94 h	140.5	89.4	0.852 ± 0.131	0.857 ± 0.132
^{103}Ru	39.26 d	497.1	90.0	0.313 ± 0.041	0.313 ± 0.041
^{105}Ru	4.44 h	724.4	47.0	0.177 ± 0.012	0.177 ± 0.012
^{105}Rh	35.36 h	319.1	19.0	0.189 ± 0.033	0.189 ± 0.033
^{112}Ag	3.13 h	617.5	43.0	0.282 ± 0.021	0.284 ± 0.021
^{113}Ag	5.37 h	298.0	43.0	0.330 ± 0.025	0.330 ± 0.025
^{117}Cd^{m}	3.36 h	1066.0	23.1	0.049 ± 0.008	
^{117}Cd^{g}	2.49 h	273.4	28.0	0.255 ± 0.037	
^{117}Cd^{total}				0.304 ± 0.037	0.304 ± 0.037
^{127}Sb	3.85 d	687.0	37.0	0.276 ± 0.033	0.276 ± 0.033
^{131}I	8.02 d	364.5	81.7	0.987 ± 0.058	0.997 ± 0.058
^{132}Te	3.2 d	228.1	88.0	1.594 ± 0.161	1.594 ± 0.161
^{133}I	20.8 h	529.9	87.0	3.255 ± 0.441	3.275 ± 0.441
^{134}Te	41.8 m	566.0	18.0	5.617 ± 0.232	5.956 ± 0.232
		767.2	29.5	4.817 ± 0.400	5.165 ± 0.400
^{135}I	6.57 h	1131.5	22.7	4.119 ± 0.441	4.140 ± 0.412
		1260.4	28.9	4.426 ± 0.045	4.449 ± 0.045
^{138}Cs^{g}	33.41 m	1435.8	76.3	7.099 ± 0.306	7.171 ± 0.306
^{139}Ba	83.03 m	165.8	76.3	8.086 ± 0.432	8.086 ± 0.432
^{140}Ba	12.75 d	537.3	24.4	6.764 ± 0.895	6.784 ± 0.898
^{141}Ce	32.5 d	145.4	48.0	6.275 ± 0.690	6.294 ± 0.692
^{142}La	91.1 m	641.3	47.0	5.812 ± 0.067	5.812 ± 0.067
^{143}Ce	33.03 h	293.3	42.8	7.042 ± 0.974	7.114 ± 0.984
^{144}Ce	284.89 d	133.5	11.09	7.414 ± 0.165	7.414 ± 0.165
^{147}Nd	10.98 d	531.0	13.1	2.842 ± 0.511	2.842 ± 0.511
^{149}Pm	53.08 h	286.0	13.1	1.989 ± 0.264	1.989 ± 0.264
^{153}Sm	46.28 h	103.2	30.0	0.445 ± 0.029	0.449 ± 0.029

Cu.Y. – Cumulative yields, M.Y. – Mass yields, ^{135}I – Fission rate monitor.

the neutron-deficient Th isotopes, ^{227}Th is the transitional region having comparable symmetric and asymmetric fission. Actinides lighter than ^{227}Th undergo symmetric fission, whereas actinides heavier than ^{227}Th undergo asymmetric fission. It has been also mentioned by them [52] that in the low energy fission, the yield of the symmetric channel strongly decreases with an increasing in mass number of the fissioning system. Thus, the yields of symmetric products in the bremsstrahlung- and neutron-induced fission of ^{232}Th are not as high as in the case of ^{227}Th. Further, the experimental work of Yoneama et al. [96] using electro-fission, i.e., the vir-

Table 2
Nuclear spectroscopic data and yields of fission products in the 10 MeV bremsstrahlung-induced fission of ^{238}U.

Nuclide	Half-life	γ-ray Energy (keV)	γ-ray Abundance (%)	Cu.Y. (%)	M.Y. (%)
^{85}Kr^{m}	4.48 h	304.9	14.0	0.781 ± 0.107	0.784 ± 0.108
^{87}Kr	76.3 m	402.6	49.6	1.609 ± 0.202	1.699 ± 0.203
^{88}Kr	2.84 h	196.3	25.9	2.771 ± 0.527	2.799 ± 0.532
^{91}Sr	9.63 h	749.8	23.6	3.780 ± 0.120	3.780 ± 0.120
		1024.3	33.0	3.858 ± 0.215	3.858 ± 0.215
^{92}Sr	2.71 h	1384.9	90.0	3.827 ± 0.452	3.846 ± 0.455
^{93}Y	10.18 h	266.9	7.3	5.467 ± 0.760	5.467 ± 0.760
^{95}Zr	64.02 d	756.7	54.0	4.558 ± 0.221	4.558 ± 0.221
^{97}Zr	16.91 h	743.4	93.0	5.433 ± 0.190	5.461 ± 0.191
^{99}Mo	65.94 h	140.5	89.4	4.835 ± 0.442	4.845 ± 0.443
^{103}Ru	39.26 d	497.1	90.0	5.239 ± 0.299	5.239 ± 0.299
^{105}Ru	4.44 h	724.4	47.0	2.571 ± 0.208	2.584 ± 0.209
^{105}Rh	35.36 h	319.1	19.0	2.626 ± 0.275	2.626 ± 0.275
^{113}Ag	5.37 h	298.0	43.0	0.155 ± 0.012	0.156 ± 0.012
^{115}Cd^{g}	53.46 h	336.2	45.9	0.102 ± 0.012	0.102 ± 0.012
^{117}Cd^{m}	3.36 h	066.0	23.1	0.007 ± 0.001	
^{117}Cd^{g}	2.49 h	273.4	28.0	0.039 ± 0.002	
^{117}Cd^{total}				0.046 ± 0.002	0.046 ± 0.002
^{127}Sb	3.85 d	687.0	37.0	0.867 ± 0.239	0.867 ± 0.239
^{129}Sb	4.44 h	812.8	43.0	1.480 ± 0.334	1.483 ± 0.335
^{131}I	8.02 d	364.5	81.7	3.511 ± 0.058	3.529 ± 0.897
^{132}Te	3.2 d	228.1	88.0	4.839 ± 0.461	4.839 ± 0.461
^{133}I	20.8 h	529.9	87.0	6.429 ± 0.801	6.442 ± 0.801
^{134}Te	41.8 m	566.0	18.0	7.602 ± 0.213	8.122 ± 0.227
		767.2	29.5	8.929 ± 0.297	9.540 ± 0.317
^{135}I	6.57 h	1131.5	22.7	5.784 ± 0.548	5.808 ± 0.550
		1260.4	28.9	5.981 ± 0.596	6.005 ± 0.598
^{138}Cs^{g}	33.41 m	1435.8	76.3	7.998 ± 0.482	8.038 ± 0.484
^{139}Ba	83.03 m	165.8	76.3	5.999 ± 0.114	5.999 ± 0.114
^{140}Ba	12.75 d	537.3	24.4	5.401 ± 0.293	5.407 ± 0.293
^{141}Ce	32.5 d	145.4	48.0	4.156 ± 0.405	4.169 ± 0.407
^{142}La	91.1 m	641.3	47.0	5.263 ± 0.520	5.263 ± 0.520
^{143}Ce	33.03 h	293.3	42.8	4.273 ± 0.292	4.294 ± 0.293
^{144}Ce	284.89 d	133.5	11.09	3.786 ± 0.269	3.786 ± 0.269
^{147}Nd	10.98 d	531.0	13.1	1.986 ± 0.197	1.986 ± 0.197
^{151}Pm	28.4 h	340.1	23.0	0.592 ± 0.072	0.592 ± 0.072

Cu.Y. – Cumulative yields, M.Y. – Mass yields, ^{135}I – Fission rate monitor.

tual photon-induced fission of ^{232}Th, also proved the triple humped fission barrier. As mentioned by them [96], the outer barrier in ^{232}Th splits into two barriers with heights of 6.5 and 5.7 MeV separated by a shallow minimum with a bottom at 5.4 MeV. They have also shown that the barrier height changes for the different vibrational states. The calculation of saddle point configurations against the mass asymmetric deformation by Moller [95] showed a different type of potential barrier for ^{232}Th compared to ^{238}U, which was mentioned before. Thus, the observation of a triple humped mass distribution from the present and earlier work in bremsstrahlung [59,60], re-

Table 3
Nuclear spectroscopic data and yields of fission products in the 10 MeV bremsstrahlung-induced fission of ^{240}Pu.

Nuclide	Half-life	γ-ray		Cu.Y. (%)	M.Y. (%)
		Energy (keV)	Abundance (%)		
^{85}Kr^{m}	4.48 h	304.9	14.0	0.827 ± 0.205	0.828 ± 0.205
^{87}Kr	76.3 m	402.6	49.6	1.329 ± 0.154	1.333 ± 0.154
^{88}Kr	2.84 h	196.3	25.9	1.447 ± 0.160	1.503 ± 0.166
^{91}Sr	9.63 h	749.8	23.6	2.603 ± 0.327	2.603 ± 0.327
		1024.3	33.0	2.579 ± 0.367	2.579 ± 0.367
^{92}Sr	2.71 h	1384.9	90.0	2.589 ± 0.350	3.599 ± 0.351
^{95}Zr	64.02 d	756.7	54.0	4.015 ± 0.834	4.027 ± 0.836
^{97}Zr	16.91 h	743.4	93.0	4.081 ± 0.526	4.102 ± 0.528
^{99}Mo	65.94 h	140.5	89.4	6.855 ± 0.986	6.855 ± 0.986
		739.8	12.13	6.780 ± 0.899	6.780 ± 0.899
^{103}Ru	39.26 d	497.1	90.0	7.746 ± 0.727	7.770 ± 0.730
^{105}Ru	4.44 h	724.4	47.0	3.848 ± 0.098	3.887 ± 0.099
^{105}Rh	35.36 h	319.1	19.0	4.078 ± 0.890	4.078 ± 0.899
^{112}Ag	3.13 h	617.5	43.0	0.530 ± 0.083	0.530 ± 0.083
^{113}Ag	5.37 h	298.0	43.0	0.374 ± 0.059	0.375 ± 0.059
^{117}Cd^{m}	3.36 h	1066.0	23.1	0.027 ± 0.005	
^{117}Cd^{g}	2.49 h	273.4	28.0	0.150 ± 0.035	
^{117}Cd^{total}				0.177 ± 0.035	0.177 ± 0.035
^{127}Sb	3.85 d	687.0	37.0	1.090 ± 0.114	1.092 ± 0.114
^{128}Sn	59.07 m	482.0	59.0	1.219 ± 0.167	1.447 ± 0.197
^{129}Sb	4.44 h	812.8	43.0	1.626 ± 0.280	1.649 ± 0.284
^{131}I	8.02 d	364.5	81.7	3.037 ± 0.607	3.037 ± 0.607
^{132}Te	3.2 d	228.1	88.0	3.539 ± 0.115	3.656 ± 0.118
^{133}I	20.8 h	529.9	87.0	5.005 ± 0.426	5.005 ± 0.426
^{134}Te	41.8 m	767.2	29.5	5.364 ± 0.197	8.065 ± 0.290
^{134}I^{g}	52.5 m	847.3	95.4	8.720 ± 0.713	8.925 ± 0.730
		884.1	54.9	7.411 ± 0.632	7.585 ± 0.647
^{135}I	6.57 h	1260.4	28.9	5.260 ± 0.172	5.524 ± 0.193
^{138}Cs^{g}	33.41 m	1435.8	76.3	6.971 ± 0.205	6.985 ± 0.205
		1009.3	29.8	6.050 ± 0.154	6.062 ± 0.154
^{139}Ba	83.03 m	165.8	76.3	5.934 ± 0.433	5.951 ± 0.434
^{140}Ba	12.75 d	537.3	24.4	5.107 ± 0.118	5.107 ± 0.118
^{141}Ce	32.5 d	145.4	48.0	4.398 ± 0.712	4.398 ± 0.714
^{142}La	91.1 m	641.3	47.0	4.519 ± 0.690	4.524 ± 0.690
^{143}Ce	33.03 h	293.3	42.8	5.001 ± 0.840	5.001 ± 0.840
^{147}Nd	10.98 d	531.0	13.1	2.429 ± 0.157	2.433 ± 0.158
^{151}Pm	28.4 h	340.1	23.0	1.026 ± 0.185	1.029 ± 0.185

Cu.Y. – Cumulative yields, M.Y. – Mass yields, ^{135}I – Fission rate monitor.

actor neutron- [14–16] and mono-energetic neutron-induced [38–42] fission of ^{232}Th compared to that of ^{238}U and ^{240}Pu is due to a different type of potential barrier. The fissioning systems in the bremsstrahlung- and neutron-induced fission of ^{232}Th differ by one neutron, which does not drastically change the observation. This is because the A/Z ratio of ^{232}Th and ^{233}Th are not very different. The effect of the A/Z ratio of the fissioning systems can be seen on the width of the mass and charge distribution due to their strong correlation with the A/Z values. This was

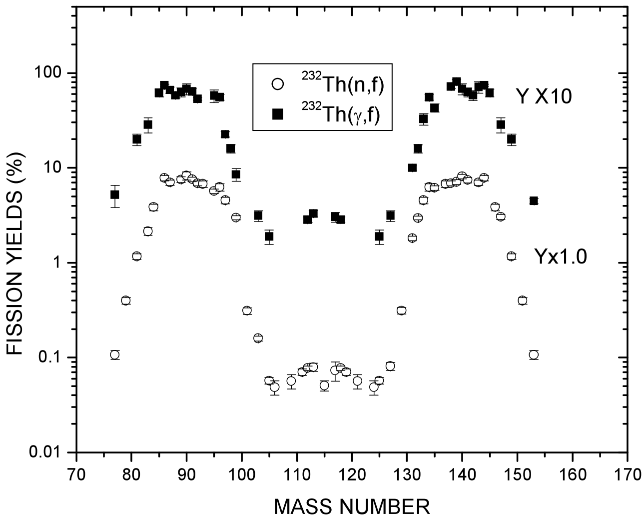

Fig. 2. Plot of yields of fission products (%) (in log scale) vs. their mass number in the bremsstrahlung- (end point energy 10 MeV) and neutron (average $E_n = 1.9$ MeV) -induced fission of ^{232}Th.

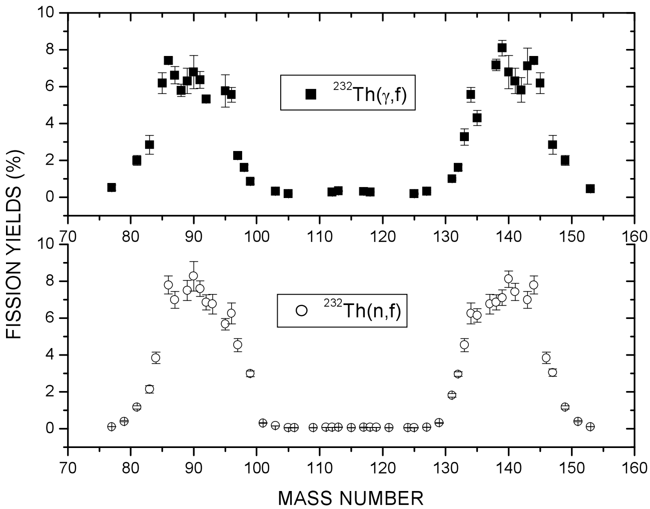

Fig. 3. Plot of yields of fission products (%) (in linear scale) vs. their mass number in the bremsstrahlung- (end point energy 10 MeV) and neutron (average $E_n = 1.9$ MeV) -induced fission of ^{232}Th.

already shown by Schmidt et al. [52] in their work on many neutron-deficient light actinides and pre-actinide fissioning systems of wide mass range variation.

Further, from Fig. 2, it can be seen that in both the bremsstrahlung- and reactor neutron-induced fission of ^{232}Th, the yields of fission products around mass numbers 133–135, 138–140, 143–145 and their complementary products are higher than other fission products. This can be clearly observed in Fig. 3, where the yields of fission products in the bremsstrahlung- and reactor neutron-induced fission of ^{232}Th were plotted on a linear scale. The higher mass yields of fission

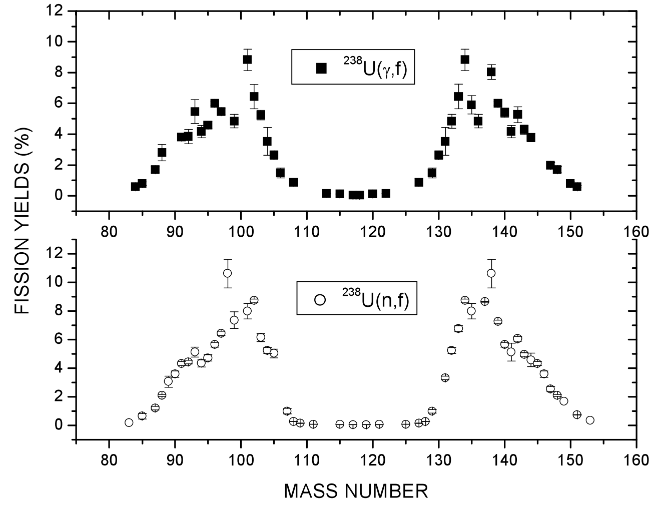

Fig. 4. Plot of yields of fission products (%) vs. their mass number in the bremsstrahlung- (end point energy 10 MeV) and neutron (average $E_n = 1.9$ MeV)-induced fission of ^{238}U.

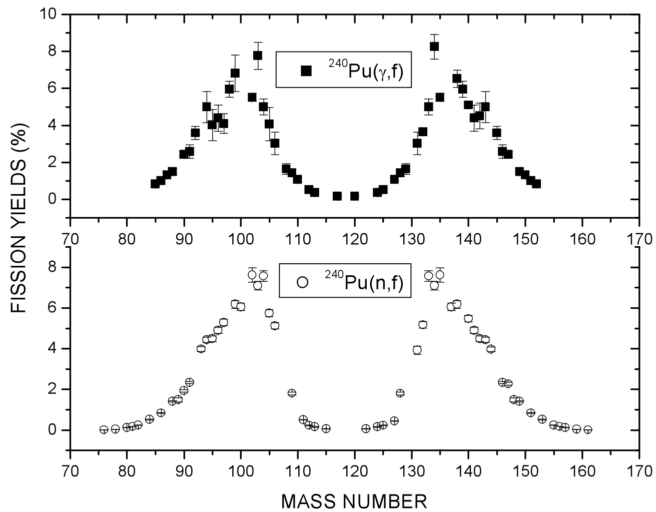

Fig. 5. Plot of yields of fission products (%) vs. their mass number in the bremsstrahlung- (end point energy 10 MeV) and neutron (average $E_n = 1.9$ MeV)-induced fission of ^{240}Pu.

products around mass numbers 133–135, 138–140, 143–145 and their complementary products were also observed in Figs. 4 and 5 in the bremsstrahlung- and reactor neutron-induced fission of ^{238}U and ^{240}Pu, respectively. Similar observations were made earlier by us [21,22] in the reactor neutron-induced fission of different actinides. As explained earlier [21,22], in the even-Z fissioning system, the peaking of mass yield in the interval of five mass units is due to even–odd effects. Since the A/Z ratio of the fission products and fissioning systems are around 2.5, the change of oscillation of mass yields occurs in the interval of five mass units. This observation is supported by the elemental profile, in which higher yields of the even-Z elements compared to adjacent odd-Z elements were shown for many neutron-deficient [52–54] and for neutron-rich even-Z actinides [91–93].

The above observation on fine structure in the asymmetric component for both even-Z and odd-Z fissioning can be explained from the point of view of the standard I and standard II channel of bimodal fission [98], which arises due to shell effects [99]. Based on standard I asymmetry, the fissioning system is characterized by spherical heavy fragment mass numbers 133–135 due to the spherical $82n$ shell and a deformed complementary light mass number. Based on standard II asymmetry, the fissioning system is characterized by a deformed heavy mass fragment near mass numbers 143–145 due to a deformed $88n$ shell and slightly deformed light mass. Thus the higher yields of fission products around mass numbers 133–135 and 143–145 in both even-Z and odd-Z fissioning systems are due to the presence of spherical $82n$ and deformed $88n$ shells, respectively. As a result an average mass of 138 ± 1 over the heavy mass region [14–22] has been observed due to higher yields of fission products around mass numbers 133–135 and 143–145. Aside from the shell effect, the N/Z value also determines the average mass and charge combination [52–54]. Thus for the average heavy mass of 138 ± 1, a corresponding average charge of 54 ± 1 is favorable from the N/Z point of view [52–54]. However, a corresponding average charge of 54 ± 1 with a fixed mass of 138 ± 1 was not observed by Benllure et al. [53] in the electromagnetic-induced fission of neutron-deficient pre-actinides and actinides. This may be because of a drastic difference in N/Z values of the neutron-deficient pre-actinides and actinides, which give rise to an increasing trend of average mass with increasing N/Z values for a fixed charge of 54 ± 1. The neutron- and bremsstrahlung-induced fission of neutron rich actinides in the present and earlier works [14–51] has an N/Z value around 1.5. Thus the higher yields of fission products around mass numbers 133–135 and 143–145 as well as average mass of 138 ± 1 with fixed charge of 54 ± 1 are expected from both shell effects [99] and the N/Z [52–54] point of view. However, shell and pairing effects decrease with an increase in excitation energy for both neutron- [38–48,51,91] and bremsstrahlung-induced [89,90] fission of actinides. In order to examine the role of excitation energy, the yields of fission products in the 10 MeV bremsstrahlung-induced fission of ^{232}Th and ^{238}U and at higher energies from Refs. [55,58,69] are plotted in Figs. 6 and 7, respectively. These data in the bremsstrahlung-induced fission of ^{232}Th and ^{238}U are based on radiochemical and/or off-line γ-ray spectrometric techniques. In the case of ^{240}Pu, there is no experimental data on fission yields based on radiochemical or off-line γ-ray spectrometric techniques, except the present data in the 10 MeV bremsstrahlung-induced fission. In view of this for the fissioning system ^{240}Pu*, the yields of fission products as a function of their mass number at different excitation energies in 10 MeV bremsstrahlung-induced fission of ^{240}Pu from present work and in the thermal [10], 6.1 MeV [51] and 14.8 MeV [33–35] neutron-induced fission of ^{239}Pu are plotted in Fig. 8. It can be seen from Figs. 6–8 that for the fissioning systems ^{232}Th*, ^{238}U* and ^{240}Pu*, the fine structure around mass numbers 133–135, 138–140, 143–145 and their complementary products decreased with an increase in excitation energy. The decreasing trend of the nuclear structure effects with an increase in excitation energy is also clear from the figure of mass yield data based on physical measurements in the bremsstrahlung-induced fission of ^{240}Pu [75]. This is supported by the decreasing trend of the nuclear structure effects with increasing neutron energy in various mono-energetic neutron-induced fissions of ^{232}Th [38–42], ^{233}U [43], ^{235}U [44,45], ^{238}U [45–48] and ^{239}Pu [38,51]. In the absence of the even–odd effect [97] in the odd-Z fissioning system, a decreasing trend of shell effect with an increase in excitation energy can be seen only in the mono-energetic neutron-induced fission of ^{237}Np [49,50].

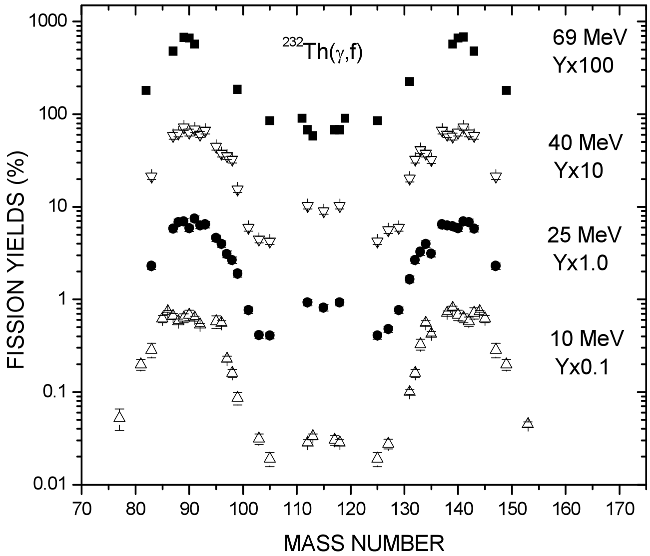

Fig. 6. Plot of yields of fission products (%) vs. their mass number in the bremsstrahlung-induced fission of ^{232}Th at different endpoint energies.

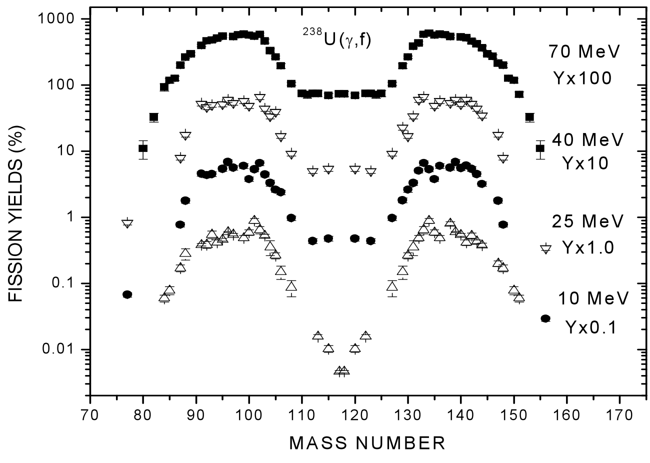

Fig. 7. Plot of yields of fission products (%) vs. their mass number in the bremsstrahlung-induced fission of ^{238}U at different endpoint energies.

Aside from the above observations, it can be also seen in Figs. 6–8 that with an increase of excitation energy, the yield of fission products in the high yield region marginally changed, whereas for the symmetric products, it significantly increased. In order to examine this aspect, the yield of fission products in the peak position, in the symmetric region and their ratio (i.e. peak-to-valley (P/V) ratio) in the bremsstrahlung-induced fission of ^{232}Th [55–60,89] and ^{238}U [61–74,90] are given in Tables 4 and 5, respectively. Similarly the yield of fission products in the peak position, the symmetric region and their ratio (i.e., peak-to-valley (P/V) ratio) in the mono-energetic neutron-induced fission of ^{232}Th [38–42] and ^{238}U [45–48] are given in Tables 6

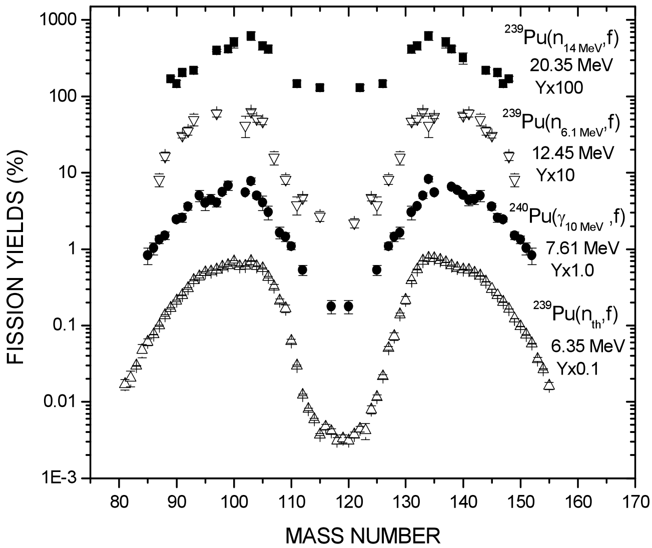

Fig. 8. Plot of yields of fission products (%) vs. their mass number at different excitation energies (E^*) in the fissioning systems ^{240}Pu* from ^{239}Pu(n_{th}, f), ^{239}Pu($n_{6.1\,\mathrm{MeV}}, f$), ^{239}Pu($n_{14.8\,\mathrm{MeV}}, f$) and ^{240}Pu ($\gamma_{10\,\mathrm{MeV}}, f$). The E^* values are mentioned inside the figure adjacent to each curve.

and 7, respectively. Since there is no data in the mono-energetic neutron-induced fission of ^{240}Pu, data on the same compound nucleus, i.e., ^{239}Pu(n, f) [51], ^{240}Pu(γ, f) [75] and ^{240}Pu(SF) [79], are given in Table 8 for comparison. Presenting these data in tabular form is necessary because in some references only the yields of asymmetric products are given at a particular energy, whereas in some other references, the yields of symmetric products are given at the same energy. In some cases, only the value of the P/V ratio is given, whereas in other cases, the yields of both symmetric and asymmetric products are given but the value of the P/V ratios is not shown. In such cases, the P/V ratio is obtained from the experimental yield data shown in Tables 4–7. The yield data of symmetric or asymmetric products given in brackets at some of the energies are the assumed values based on the systematic increasing or decreasing trend of yields at adjacent energies. This was done to evaluate the P/V ratio and examine its trend in a wide range of bremsstrahlung and neutron energies.

The experimental yield of symmetric and high yield asymmetric fission products from Tables 4–7 in the bremsstrahlung- and mono-energetic neutron-induced fission of ^{232}Th and ^{238}U are plotted in Figs. 9 and 10. The peak-to-valley (P/V) ratios in the bremsstrahlung- and neutron-induced fission of ^{232}Th and ^{238}U from Tables 4 and 5 are plotted in Figs. 11 and 12 as a function of excitation energy up to 24 MeV for comparison. From Figs. 9 and 10, a marginal decrease of high yield fission products with an increase in bremsstrahlung and neutron energy is clearly seen. However, the yield of symmetric fission products increased sharply in the beginning up to a certain energy, where second chance fission starts. Thereafter, the increasing trend is slow with an increase of bremsstrahlung- and mono-energetic neutron energy. Accordingly, the P/V ratio decreases with an increase of excitation energy, which can be seen from Figs. 11 and 12 for the bremsstrahlung- and neutron-induced fission of ^{232}Th and ^{238}U, respectively. These observations indicate the role of excitation energy on fission yields and their P/V ratio in the bremsstrahlung- and neutron-induced fission of actinides.

Table 4
Yields of asymmetric (Y_a) and symmetric (Y_s) products and P/V ratio in bremsstrahlung-induced fission of ^{232}Th.

E_γ (MeV)	E^* (MeV)	Y_a (%)	Y_s (%)	P/V ratio	Ref.
6.50	6.02	8.609 ± 0.431	–	–	[87]
7.00	6.23	8.435 ± 0.422	–	–	[87]
8.0 (7.33)	6.52 (6.34)	8.005 ± 0.400	<0.008	696.1 ± 214.7	[87,60]
			<0.015		[60]
9.0 (8.35)	6.86 (6.64)	8.530 ± 0.410	0.090 ± 0.030	85.3 ± 21.7	[59,60]
			0.110 ± 0.020		[60]
9.31	6.97	(8.308 ± 0.415)	0.250 ± 0.050	38.6 ± 6.6	[60]
			0.180 ± 0.020		[60]
10.0	7.35	8.086 ± 0.432	0.304 ± 0.032	26.6 ± 3.5	A
11.0	7.75	8.766 ± 0.438	–	–	[87]
12.0 (11.13)	8.35 (7.84)	7.779 ± 0.389	0.650 ± 0.100	13.5 ± 1.9	[87,60]
			0.500 ± 0.020		[60]
14.0	9.44	7.852 ± 0.393	(0.725 ± 0.036)	10.8 ± 0.8	[87,60]
15.0	10.5	7.890 ± 0.610	(0.810 ± 0.041)	9.7 ± 0.9	[59,60]
25.0	13.22	7.440 ± 0.595	0.813 ± 0.065	8.0	[58]
25.0	13.22	–	0.870 ± 0.120	–	[56]
30.0	13.75	7.350 ± 0.588	0.871 ± 0.070	7.6	[58]
35.0	14.7	7.810 ± 0.625	0.905 ± 0.072	6.9	[58]
38.0	15.39	7.300 ± 0.420	–	–	[59]
40.0	15.87	7.280 ± 0.582	0.904 ± 0.072	6.6	[58]
69.0	21.24	6.800 ± 0.499	(1.200 ± 0.096)	5.7 ± 0.7	[55,60]

A – Present work. Yield of fission products given in brackets is extrapolated value from Refs. [60] and [87].

Table 5
Yields of asymmetric (Y_a) and symmetric (Y_s) products and P/V ratio in bremsstrahlung-induced fission of ^{238}U.

E_γ (MeV)	E^* (MeV)	Y_a (%)	Y_s (%)	P/V ratio	Ref.
6.12	5.66	8.570 ± 0.429	–	–	[88]
6.44	5.84	8.340 ± 0.417	–	–	[88]
7.33	6.23	8.380 ± 0.419	–	–	[88]
8.35	6.68	8.430 ± 0.422	–	–	[88]
9.0	6.86	7.140 ± 0.660	0.023 ± 0.006	310.4 ± 85.9	[61]
9.31	7.19	7.690 ± 0.385	–	–	[88]
10.0	7.55	6.800 ± 0.600	0.033 ± 0.007	206.9 ± 47.7	[61,62]
10.0	7.55	8.821 ± 0.709	0.046 ± 0.002	192.0 ± 17.5	A
11.0	8.40	7.730 ± 0.387	–	–	[88]
12.0	9.70	6.880 ± 0.230	0.075 ± 0.007	78.0 ± 7.0	[69]
15.0	11.87	6.870 ± 0.250	0.172 ± 0.021	31.0 ± 2.0	[69]
16.0	12.4	6.600	0.173 ± 0.010	38.0	[61]
20.0	13.4	6.840 ± 0.220	0.281 ± 0.031	24.3 ± 2.8	[69]
21.0	13.6	6.600	0.268 ± 0.010	23.0	[61]
22.0	13.85	6.900 ± 0.500	0.315 ± 0.055	20.0	[61,66]
25.0	14.38	6.590 ± 0.330	0.334 ± 0.032	19.0 ± 2.0	[68]
25.0	14.38	–	0.440 ± 0.060	–	[56]
25.0	14.38	6.870 ± 0.550	0.475 ± 0.038	16.0 ± 0.5	[58,71]
30.0	14.7	6.430 ± 0.210	0.446 ± 0.045	13.0 ± 0.5	[69]
30.0	14.7	6.610 ± 0.529	0.522 ± 0.042	12.0	[58]
35.0	15.08	6.180 ± 0.494	0.529 ± 0.042	11.4	[58]
40.0	15.08	6.020 ± 0.482	0.542 ± 0.043	10.6	[58]
48.0	16.22	6.200 ± 0.300	0.600 ± 0.020	11.0	[61]
70.0	19.9	6.120 ± 0.270	0.737 ± 0.064	8.5 ± 0.3	[69]

A – Present work.

Table 6
Yields of asymmetric (Y_a) and symmetric (Y_s) products and P/V ratio in neutron-induced fission of ^{232}Th.

E_n (MeV)	E^* (MeV)	Y_a (%)	Y_s (%)	P/V ratio	Ref.
1.60 ± 0.02	6.21	–	–	218.9 ± 47.7	[40]
1.68 ± 0.02	6.29	–	–	205.1 ± 42.1	[40]
1.72 ± 0.02	6.33	–	–	292.7 ± 73.2	[40]
1.77 ± 0.02	6.38	–	–	241.5 ± 58.8	[40]
1.88 ± 0.02	6.49	–	–	238.2 ± 36.5	[40]
2.00 ± 0.02	6.61	–	–	283.5 ± 64.9	[40]
2.00	6.61	8.950 ± 0.250	0.005 ± 0.001	–	[41]
2.20 ± 0.02	6.81	–	–	212.3 ± 53.9	[40]
2.43 ± 0.02	7.04	–	–	214.5 ± 35.6	[40]
2.96 ± 0.41	7.57	–	–	118.5 ± 17.5	[40]
2.97	7.58	–	–	122.0	[39]
3.00	7.61	8.600 ± 0.230	0.023 ± 0.004	–	[41]
3.00	7.61	7.890 ± 0.094	0.045 ± 0.009	–	[23]
3.10 ± 0.15	7.71	–	–	63.0 ± 11.0	[42]
4.00	8.61	8.010 ± 0.200	0.099 ± 0.015	80.9 ± 12.3	[41]
4.03 ± 0.02	8.64	–	–	71.0	[39]
4.20 ± 0.11	8.81	–	–	27.2 ± 3.1	[40]
4.81 ± 0.02	9.52	–	–	51.0	[39]
5.20 ± 0.25	9.87	–	–	29.0 ± 3.0	[42]
5.30 ± 0.11	9.91	–	–	26.4 ± 2.1	[40]
5.90	10.51	7.750 ± 0.550	0.270 ± 0.040	28.7 ± 4.7	[41]
6.40	11.01	8.080 ± 0.230	0.230 ± 0.040	35.1 ± 6.1	[41]
6.90	11.51	8.700 ± 0.340	0.200 ± 0.030	43.5 ± 6.7	[41]
7.60	12.21	8.380 ± 0.230	0.200 ± 0.030	41.9 ± 6.4	[41]
8.00	12.61	7.870 ± 0.350	0.290 ± 0.030	27.1 ± 3.9	[41]
9.10 ± 0.30	13.71	(8.000 ± 0.500)	0.436 ± 0.014	18.3 ± 1.27	[38]
11.00	15.61	8.100 ± 0.900	0.760 ± 0.015	10.7 ± 1.30	[23]
13.40 ± 0.17	18.01	(8.000 ± 0.500)	1.440 ± 0.020	5.6 ± 0.36	[38]
14.00 ± 0.06	18.61	(7.500 ± 0.500)	1.200 ± 0.100	4.79 ± 0.06	[25]
14.10 ± 0.16	18.71	(7.500 ± 0.500)	1.340 ± 0.02	$0\ 5.6 \pm 0.38$	[38]
14.80 ± 0.80	19.41	6.500 ± 0.325	1.240 ± 0.200	5.2 ± 0.89	[23–27]
14.90 ± 0.25	19.51	(6.500 ± 0.500)	1.280 ± 0.040	5.1 ± 0.42	[38]
18.10 ± 0.25	22.71	(6.500 ± 0.500)	1.920 ± 0.100	3.4 ± 0.31	[38]

Yield of fission products given in brackets are assumed value.

Further, it can be seen in Figs. 9–12 that the increasing trend of symmetric fission yield and decreasing trend of P/V ratio is not similar in the bremsstrahlung- and neutron-induced fission of ^{232}Th and ^{238}U. In both fission events of ^{232}Th and ^{238}U (Figs. 9 and 10), the symmetric yields increased sharply up to the excitation energy of 9–10 MeV and then slowly up to 14 MeV. Thereafter, it remained almost constant up to the excitation energy of 22 MeV. A decreasing trend of P/V ratio in the bremsstrahlung- and mono-energetic neutron-induced fission of ^{232}Th and ^{238}U also followed similar trends, as shown in Figs. 11 and 12, respectively. This was due to the increase of multi-chance fission probabilities beyond 9–14 MeV, which arises from pre-fission neutron emission. When the excitation energy exceeds the neutron binding energy of the compound nucleus, second chance fission starts, where fission occurs from the residual nucleus at a lower excitation energy. However, the different trends of symmetric yields and P/V ratios in bremsstrahlung- and neutron-induced fission of ^{232}Th and ^{238}U depend on the availability of excitation energy and the intrinsic degree of freedom, which depends upon the nuclear viscosity,

Table 7
Yields of asymmetric (Y_a) and symmetric (Y_s) products and P/V ratio in neutron-induced fission of ^{238}U.

E_n (MeV)	E^* (MeV)	Y_a (%)	Y_s (%)	P/V ratio	Ref.
1.5	5.85	8.120 ± 0.40	0.0102 ± 0.0014	796.1 ± 116.1	[46]
1.5	5.85	–	0.0075 ± 0.0008	825.0	[47,46]
1.72	6.07	7.350 ± 0.770	–	–	[48]
2.0	6.35	7.780 ± 0.370	0.0121 ± 0.0017	643.0 ± 95.4	[46]
2.0	6.35	–	0.0135 ± 0.0014	452.0	[47,46]
2.16	6.55	7.510 ± 0.830	–	–	[48]
3.0	7.35	–	0.026 ± 0.003	238.0	[47,46]
3.0	7.35	8.190 ± 0.840	0.034 ± 0.006	240.9 ± 49.2	[28]
3.72	8.07	7.120 ± 0.940	–	–	[48]
3.9	8.25	7.760 ± 0.420	0.034 ± 0.005	228.2 ± 35.8	[46]
3.9	8.25	–	0.047 ± 0.005	129.0	[47,46]
4.78	9.13	6.770 ± 0.700	–	–	[48]
4.8	9.15	–	0.068 ± 0.007	89.0	[47,46]
5.5	9.85	7.000 ± 0.500	0.077 ± 0.011	90.9 ± 14.5	[46]
5.98	10.33	6.290 ± 0.800	–	–	[48]
6.0	10.35	6.132 ± 0.699	0.124 ± 0.010	49.5 ± 6.9	4[5]
6.9	11.25	7.240 ± 0.860	0.134 ± 0.018	54.0 ± 9.7	[46]
7.1	11.45	6.839 ± 0.595	0.121 ± 0.009	56.5 ± 6.5	[45]
7.7	12.05	7.020 ± 0.430	0.191 ± 0.032	36.8 ± 6.6	[46]
8.1	12.45	6.713 ± 0.665	0.135 ± 0.011	49.7 ± 6.4	[45]
9.1	13.45	6.308 ± 0.688	0.191 ± 0.016	33.0 ± 4.5	[45]
13.0	17.35	–	0.570 ± 0.070	8.8	[47,46]
14.0	18.10	6.190 ± 0.350	0.860 ± 0.090	7.2 ± 0.9	[26,31]
14.8	19.15	6.350 ± 0.300	0.870 ± 0.150	7.3 ± 1.3	[30]
14.9	19.25	–	0.800 ± 0.160	–	[38]
15.0	19.35	–	0.780 ± 0.090	6.5	[47,46]
16.4	20.75	–	0.870 ± 0.100	5.8	[47,46]
17.7	22.05	–	0.740 ± 0.090	6.8	[47,46]

i.e., coupling between collective and intrinsic degrees of freedom. This is clearly reflected in the even–odd effect in the bremsstrahlung- [89,90] and neutron-induced [91] fission of ^{232}Th and ^{238}U. The availability of lower intrinsic excitation energy in Th compared to U causes a higher even–odd effect in the former case than in the latter [89–91]. These observations indicate the role of excitation energy in addition to the qualitative picture of sharing excitation energy between the intrinsic and collective degrees of freedom depending on nuclear viscosity, which is different for different actinides. From the above discussion, it is also clear that ^{232}Th behaves in a slightly different way than ^{238}U in both bremsstrahlung- and neutron-induced fission. This may also be due to different type of potential barrier for ^{232}Th compared to other actinides in addition to differences in nuclear viscosity. Thus the P/V ratios in the bremsstrahlung- and neutron-induced fission of ^{232}Th are always lower than those of ^{238}U and ^{240}Pu (Fig. 11).

Other than the above observations, the role of incomplete/non-compound energy mixing in the bremsstrahlung-induced fission compared to mono-energetic neutron-induced fission can be examined by comparing the P/V ratios in the bremsstrahlung-induced fission of ^{240}Pu [75] with that of neutron-induced fission of ^{239}Pu [51]. For this purpose, the P/V ratios in the neutron-induced fission of ^{239}Pu [51], spontaneous and bremsstrahlung-induced fission of ^{240}Pu from the literature [75] and present work are plotted in Fig. 13. It can be seen from Fig. 13 that for the compound nucleus ^{240}Pu* at the same excitation energy, the bremsstrahlung-induced

Table 8
Yields of asymmetric (Y_a) and symmetric (Y_s) products and P/V ratio in the fission system ^{240}Pu.

E (MeV)	E^* (MeV)	Y_a (%)	Y_s (%)	P/V ratio	Ref.
^{240}Pu(SF)					
0	0	8.190 ± 0.120	–	400.0 ± 180.0	[51,79]
^{239}Pu(n, f)					
0.025E–06	6.53	7.667 ± 0.054	0.031 ± 0.003	247.3 ± 24.0	[10]
0.17	6.70	7.640 ± 0.450	0.032 ± 0.005	230.0	[51]
			0.027 ± 0.004		[51]
1.0	7.53	7.020 ± 0.410	0.044 ± 0.007	160.0	[51]
			0.036 ± 0.005		[51]
2.0	8.53	7.320 ± 0.430	0.048 ± 0.007	130.0	[51]
			0.050 ± 0.008		[51]
3.4	9.93	7.060 ± 0.410	0.085 ± 0.013	70.0	[51]
			0.110 ± 0.020		[51]
4.5	11.03	7.090 ± 0.420	0.130 ± 0.020	50.0	[51]
6.1	12.63	6.300 ± 0.370	0.220 ± 0.030	25.0	[51]
			0.270 ± 0.040		[51]
	7.9	14.43	6.240 ± 0.360	– 13.0	[51]
14.5	21.03	6.250 ± 0.800	1.300 ± 0.110	4.9 ± 0.5	[34]
14.7	21.23	–	–	2.95 ± 0.35	[33]
^{240}Pu(γ, f)					
10.0	7.61	8.255 ± 0.670	0.177 ± 0.035	46.6 ± 10.0	A
12.0	9.40	–	–	27.0 ± 3.0	[75]
15.0	11.30	–	–	20.6 ± 1.3	[75]
20.0	12.60	–	–	13.1 ± 0.4	[75]
30.0	13.30	–	–	9.3 ± 0.3	[75]

A – Present work.

fission of ^{240}Pu had a lower P/V ratio than the mono-energetic neutron-induced fission of ^{239}Pu. The observation of lower P/V ratios at the same excitation energy for reactor neutron-induced fission compared to the mono-energetic neutron-induced fission of ^{232}Th [14–16], ^{238}U [21, 22] and ^{237}Np [17,18,22] support the above claim. The observation of lower P/V ratios in the fission of actinides induced by bremsstrahlung or reactor neutrons compared to mono-energetic neutrons or photons is most likely due to contribution of the high energy photons or neutrons to the symmetric part in the former case. This observation can be confirmed by comparing the data on mono-energetic photon- and bremsstrahlung-induced fission of the same actinides. However, fission yield data in the mono-energetic photon-induced fission of actinides are available only for ^{238}U [64], where the P/V ratio is not given. In addition to this, there are no data on fission yields for the mono-energetic photon-induced fission of other actinides. This is due to the fact that mono-energetic photon beams are not easily available.

5. Conclusions

(i) The yields of fission products in the 10 MeV bremsstrahlung-induced fission of ^{240}Pu were determined for the first time using off-line γ-ray spectrometric techniques.
(ii) In the bremsstrahlung- and neutron-induced fission of ^{232}Th, ^{238}U and ^{240}Pu, the yields of fission products around mass numbers 133–135, 138–140 and 143–145 as well as their complementary products were higher due to nuclear structure (shell and/or even–odd) effects and favorable N/Z values.

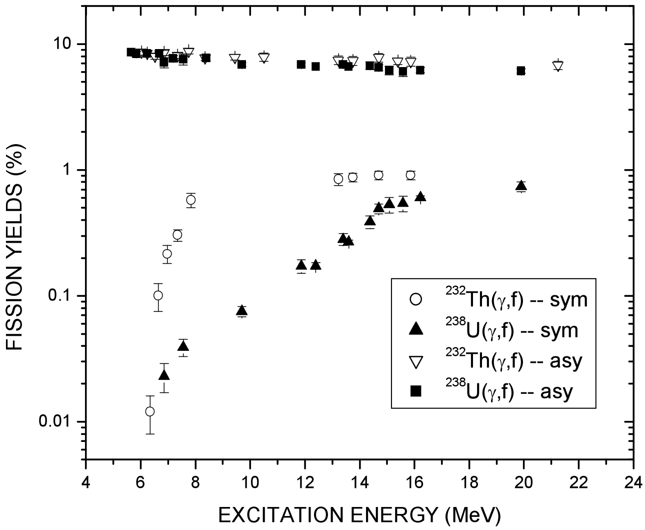

Fig. 9. Plot of yields of symmetric and asymmetric fission products (%) in the bremsstrahlung-induced fission of ^{232}Th and ^{238}U as a function of excitation energy.

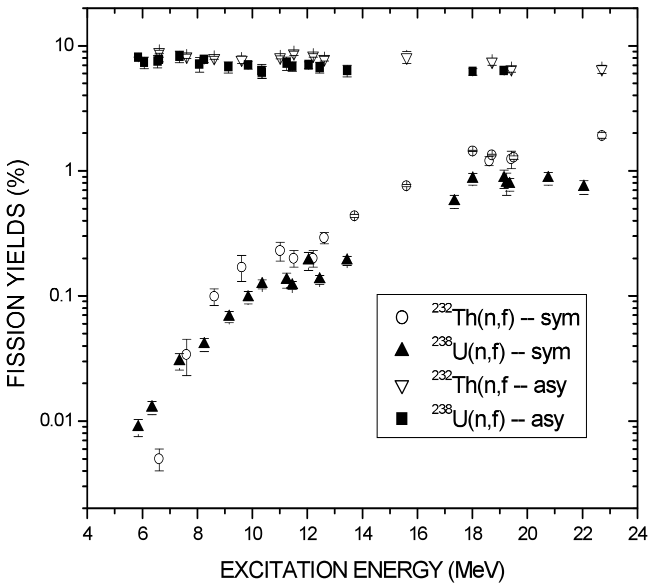

Fig. 10. Plot of yields of symmetric and asymmetric fission products (%) in the neutron-induced fission of ^{232}Th and ^{238}U as a function of excitation energy.

(iii) In the bremsstrahlung- and neutron-induced fission of actinides, the yields of asymmetric products marginally decreased, whereas for symmetric products it increased sharply up to the excitation energy of 9–14 MeV. Thereafter, it varied slowly due to pre-fission neutron emission and an increase in multi-chance fission probability. The decreasing trend of P/V ratio follows accordingly with an increase in excitation energy.

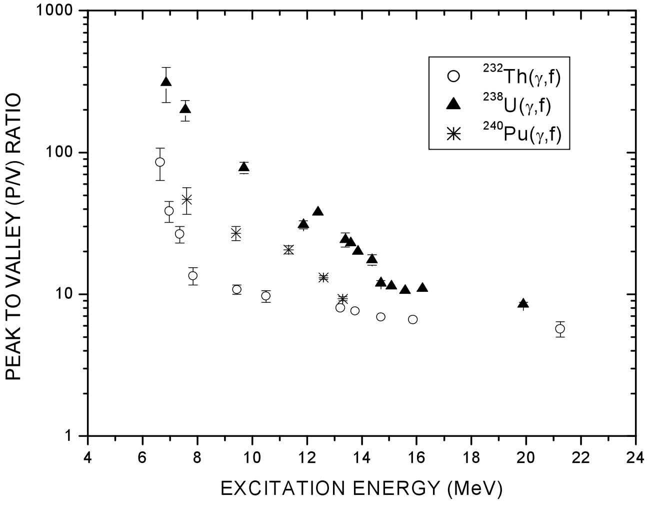

Fig. 11. Plot of peak to valley (P/V) ratio as a function of excitation energy in the 6–70 MeV bremsstrahlung-induced fission of ^{232}Th, ^{238}U and ^{240}Pu.

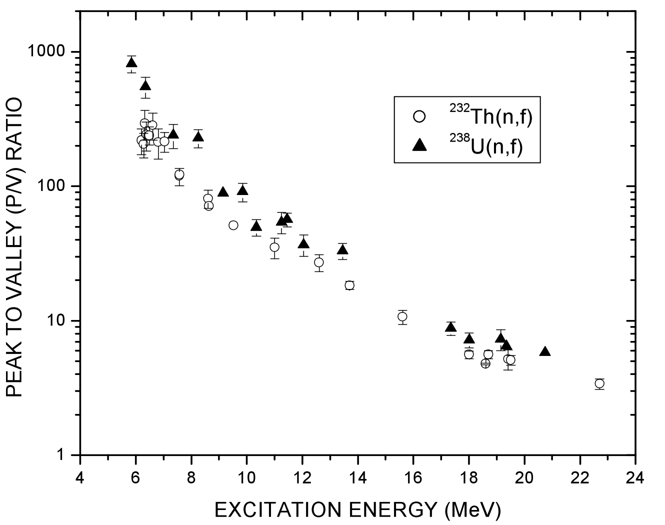

Fig. 12. Plot of peak to valley (P/V) ratio as a function of excitation energy in the neutron-induced fission of ^{232}Th and ^{238}U.

(iv) The peak to valley (P/V) ratio at all excitation energies is always lower for ^{232}Th than ^{238}U and ^{240}Pu due to the presence of a third peak in the symmetric mass region. This is due to the different types of potential barrier for ^{232}Th.

(v) The increase of symmetric yield and decrease of P/V ratio also behave differently in the bremsstrahlung- and neutron-induced fission of ^{232}Th compared to ^{238}U. This indicates that the availability of intrinsic excitation energy is different for different actinides depending on the coupling between the collective and intrinsic degrees of freedom.

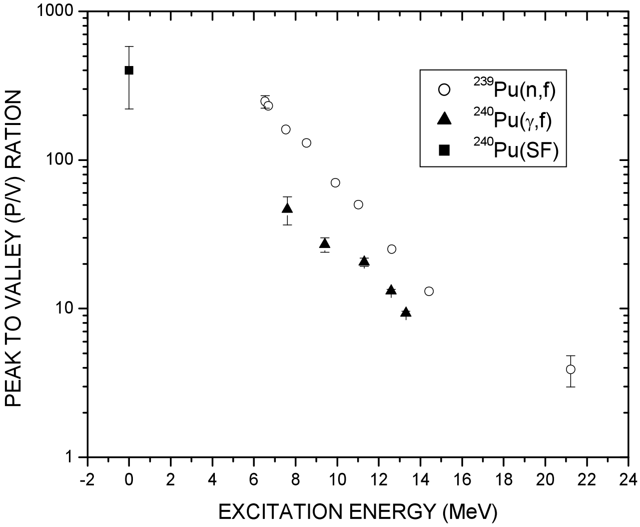

Fig. 13. Plot of peak to valley (P/V) ratio as a function of excitation energy in the compound nuclei ^{240}Pu* from ^{240}Pu(SF), ^{240}Pu(γ, f) and ^{239}Pu(n, f).

(vi) The P/V ratios at all excitation energies are always lower in bremsstrahlung-induced fission compared to mono-energetic neutron-induced fission of actinides. This effect indicates incomplete/non-compound energy mixing in the former compared with the latter case.

Acknowledgement

The authors are thankful to the staff of electron LINAC at EBC, Kharghar, Navi-Mumbai and Dr. L.M. Gantayet, Associate Director of the BTD group, BARC for providing the electron beam to carry out the experiments. We are highly indebted to the referees and editorial office for their constructive comments for improvement of the manuscript as well as for English corrections.

References

[1] T.R. Allen, D.C. Crawford, Science and Technology of Nuclear Installations 2007 (2007), Article ID 97486.
[2] Annual Project Status Report 2000, MIT-ANP-PR-071, INEFL/EXT-2009-00994.
[3] S. Ganesan, Creation of Indian experimental benchmarks for thorium fuel cycle, IAEA Coordinated research project on “Evaluated data for thorium–uranium fuel cycle”, in: Third Research Co-ordination Meeting, 30 January to 2 February 2006, Vienna, Austria, INDC (NDS)-0494, 2006.
[4] C. Rubia, et al., CERN/AT/95-44 (ET), CERN/AT/95-53 (ET), CERN/LHC/96-01 (LET), CERN/LHC/97-01 (EET).
[5] Accelerator driven system energy generation and transmutation of nuclear waste. Status report IAEA-TECDO-985, Nov. 1997.
[6] K. Oyamatsu, H. Takeuchi, M. Sagisaka, J. Katakura, J. Nucl. Sci. Techol. 38 (2001) 477.
[7] C. Wagemans, The Nuclear Fission Process, CRC Press, London, 1990.
[8] R. Vandenbosch, J.R. Huizenga, Nuclear Fission, Academic Press, New York, 1973.
[9] E.K. Hyde, The Nuclear Properties of the Heavy Elements, vol. III. Fission Phenomenon, Dover Publication Inc., New York, 1971.
[10] B.F. Rider, Compilation of fission products yields, NEDO, 12154 3c ENDF-327, Valecicecitos Nuclear Centre, 1981.
[11] J.R. England, B.F. Rider, Evaluation and compilation of fission products yields, ENDF/B-VI, 1989, 1992.

[12] M. James, R. Mills, Neutron fission products yields, UKFY2, 1991; JEF-2.2, 1993.
[13] A.C. Wahl, Atomic Data Nucl. Data Tables 39 (1988) 1.
[14] H.N. Erten, A. Grutter, E. Rossler, H.R. von Gunten, Nucl. Sci. Eng. 79 (1981) 167.
[15] R.H. Iyer, C.K. Mathews, N. Ravindran, K. Rengan, D.V. Singh, M.V. Ramaniah, H.D. Sharma, J. Inorg. Nucl. Chem. 25 (1963) 465.
[16] A. Turkevich, J.B. Nidday, Phys. Rev. 84 (1951) 52.
[17] M.N. Namboodiri, N. Ravindran, M. Rajagopalan, M.V. Ramaniah, J. Inorg. Nucl. Chem. 30 (1968) 2305.
[18] R. Stella, L.G. Moretto, V. Maxia, M. Di Casa, V. Crespi, M.A. Rollier, J. Inorg. Nucl. Chem. 31 (1969) 3739.
[19] W.A. Myers, M.V. Kantelo, R.L. Osborne, A.L. Prindlen, D.R. Nethaway, Phys. Rev. C 18 (1978) 1700.
[20] R.A. Sigg, M.V. Kantelo, D.H. Sisson, A.L. Prindle, D.R. Nethaway, Phys. Rev. C 27 (1983) 245.
[21] H. Naik, A.G.C. Nair, P.C. Kalsi, A.K. Pandey, R.J. Singh, A. Ramaswami, R.H. Iyer, Radiochim. Acta 75 (1996) 69.
[22] R.H. Iyer, H. Naik, A.K. Pandey, P.C. Kalsi, R.J. Singh, A. Ramaswami, A.G.C. Nair, Nucl. Sci. Eng. 135 (2000) 227.
[23] K.M. Broom, Phys. Rev. 133 (1964) 874.
[24] R. Ganapathy, P.K. Kuroda, J. Inorg. Nucl. Chem. 28 (1966) 2071.
[25] Tin Mo, M.N. Rao, J. Inorg. Nucl. Chem. 30 (1968) 345.
[26] L.H. Gevaert, R.E. Jervis, H.D. Sharma, Can. J. Chem. 48 (1970) 641.
[27] D.L. Swindle, D.T. Moore, J.N. Beck, P.K. Kuroda, J. Inorg. Nucl. Chem. 33 (1971) 3643.
[28] J.T. Harvey, D.E. Adams, W.D. James, J.N. Beck, J.L. Meason, P.K. Kuroda, J. Inorg. Nucl. Chem. 37 (1975) 2243.
[29] D.R. Nethaway, B. Mendoza, Phys. Rev. C 6 (1972) 1821, 1827.
[30] D.E. Adams, W.D. James, J.N. Beck, P.K. Kuroda, J. Inorg. Nucl. Chem. 37 (1975) 419.
[31] M. Rajagopalan, H.S. Pruys, A. Grutter, E.A. Hermes, H.R. von Gunten, J. Inorg. Nucl. Chem. 38 (1976) 351.
[32] W.D. James, D.E. Adams, J.N. Beck, P.K. Kuroda, J. Inorg. Nucl. Chem. 37 (1975) 1341.
[33] J.G. Cunninghame, K. Fritze, J.E. Lynn, C.B. Webster, Nucl. Phys. 84 (1966) 49.
[34] E.K. Bonyushkan, Yu.S. Zamyatnin, V.V. Spektor, V.V. Rachevr, V.R. Negina, V.N. Zamyatnina, Sov. J. At. Energy 10 (1961) 10.
[35] D.R. Nethaway, A.L. Prindle, W.A. Mayers, W.C. Fuqua, A.V. Kantelo, Phys. Rev. C 16 (1977) 1907.
[36] A.L. Prindle, D.H. Sisson, D.R. Nethaway, M.V. Kantelo, R.A. Sigg, Phys. Rev. C 20 (1979) 1824.
[37] I. Winkelmann, D.C. Aumann, Phys. Rev. C 30 (1984) 934.
[38] G.P. Ford, R.B. Leachman, Phys. Rev. B 137 (1965) 826.
[39] W. Holubarsch, L. Pfeiffer, F. Gonnenwein, Nucl. Phys. A 171 (1971) 631.
[40] J. Trochon, H. Abou Yehia, F. Brisard, Y. Pranal, Nucl. Phys. A 318 (1979) 63.
[41] L.E. Glendenin, J.E. Gindler, I. Ahmad, D.J. Henderson, J.W. Meadows, Phys. Rev. C 22 (1980) 152.
[42] S.T. Lam, L.L. Yu, H.W. Fielding, W.K. Dawson, G.C. Neilson, Phys. Rev. C 28 (1983) 1212.
[43] V.I. Senchenko, A.S. Sergachev, V.B. Mikhailov, V.G. Vorob'eva, M.Z. Tarasko, B.D. Kuz'minov, Sov. J. Nucl. Phys. 6 (1967) 516.
[44] L.E. Glendenin, J.E. Gindler, D.J. Henderson, J.W. Meadows, Phys. Rev. C 24 (1981) 2600.
[45] T.C. Chapman, G. A Anzelon, G.C. Spitale, D.R. Nethaway, Phys. Rev. C 17 (1978) 1089.
[46] S. Nagy, K.F. Flynn, J.E. Gindler, J.W. Meadows, L.E. Glendenin, Phys. Rev. C 17 (1978) 163.
[47] N.L. Borisova, S.M. Dubrovina, V.I. Novgorodtseva, V.A. Pchelin, V.A. Shigin, V.M. Shubko, Sov. J. Nucl. Phys. 6 (1968) 331.
[48] A. Afarideh, K. Randle Annole, Ann. Nucl. Energy 16 (1989) 313.
[49] A.A. Naqvi, F. Kappeler, F. Dickman, R. Muller, Phys. Rev. C 34 (1986) 218.
[50] F.-J. Hambsch, F. Vives, P. Siegler, S. Oberstedt, Nucl. Phys. A 679 (2000) 3.
[51] J.E. Gindler, L.E. Glendenin, D.J. Henderson, J.W. Meadows, Phys. Rev. C 27 (1983) 2058.
[52] K.-H. Schmidt, S. Steinhauser, C. Bockstiegel, A. Rewe, A. Heinz, A.R. Junghans, J. Benlliure, H.-G. Clerc, M. de Jong, J. Muller, M. Pfutzner, B. Voss, Nucl. Phys. A 665 (2000) 221.
[53] S. Steinhauser, J. Benlliure, C. Bockstiegel, H.-G. Clerc, A. Heinz, A. Rewe, M. de Jong, A.R. Junghans, J. Muller, M. Pfutzner, K.-H. Schmidt, Nucl. Phys. A 634 (20) (1998) 89.
[54] J. Benlliure, A.R. Junghans, K.-H. Schmidt, Eur. Phys. J. A 13 (2002) 93.
[55] D.M. Hiller, D.S. Martin Jr., Phys. Rev. 90 (1953) 581.
[56] L.H. Gevaert, R.E. Jervis, S.C. Subbarao, H.D. Sharma, Can. J. Chem. 48 (1970) 652.
[57] B. Schroder, G. Nydahl, B. Forkman, Nucl. Phys. A 143 (1970) 449.
[58] A. Chattopadhyay, K.A. Dost, I. Krajbich, H.D. Sharma, J. Inorg. Nucl. Chem. 35 (1973) 2621.
[59] J.C. Hogan, A.E. Richardson, J.L. Meason, H.L. Wright, Phys. Rev. C 16 (1977) 2296.

[60] M. Piessens, E. Jacobs, S. Pomme, D. De Frenne, Nucl. Phys. A 556 (1993) 88.
[61] R.A. Schmitt, N. Sugarman, Phys. Rev. 95 (1954) 1260.
[62] H.G. Richter, C.D. Coryell, Phys. Rev. 95 (1954) 1550.
[63] L. Katz, T.M. Kavanagh, A.G.W. Cameron, E.C. Bailey, J.W.T. Spinks, Phys. Rev. 99 (1958) 98.
[64] J.L. Meason, P.K. Kuroda, Phys. Rev. 142 (1966) 691.
[65] I.R. Willams, C.B. Fulmer, G.F. Dell, M.J. Engebretson, Phys. Lett. B 26 (1968) 140.
[66] D. Swindle, R. Wright, K. Takahashi, W.H. Rivera, L. Meason, Nucl. Sci. Eng. 52 (1973) 466.
[67] W.D. James, D.E. Adams, R.A. Sigg, J.T. Harvey, J.L. Meason, J.N. Beck, P.K. Kuroda, H.L. Wright, J.C. Hogan, J. Inorg. Nucl. Chem. 38 (1978) 1100.
[68] H. Thierens, D. De Frenne, E. Jacobs, A. De Clercq, P. D'Hondt, A.J. Deruytter, Phys. Rev. C 14 (1976) 1058.
[69] E. Jacobs, H. Thierens, A. De Frenne, A. De Clercq, P. D'Hondt, P. De Gelder, A.J. Deruytter, Phys. Rev. C 19 (1979) 422.
[70] E. Jacobs, H. Thierens, D. De Frenne, A. De Clercq, P. D'Hondt, P. De Gelder, A.J. Deruytter, Phys. Rev. C 21 (1980) 237.
[71] A. De Clercq, E. Jacobs, D. De Frenne, H. Thirens, P. D'Hondt, A.J. Deruytter, Phys. Rev. C 13 (1976) 1536.
[72] E. Jacobs, A. De Clercq, H. Thierens, D. De Frenne, P. D'Hondt, P. De Gelder, A.J. Deruytter, Phys. Rev. C 20 (1979) 2249.
[73] S. Pomme, E. Jacobs, M. Piessens, D. De Frenne, K. Persyn, K. Govaert, N.-L. Yoneama, Nucl. Phys. A 572 (1994) 237.
[74] K. Persyn, E. Jacobs, S. Pomme, D. De Frenne, K. Govaert, M.-L. Yoneama, Nucl. Phys. A 615 (1997) 198.
[75] H. Thierens, A. De Clercq, E. Jacobs, D. De Frenne, P. D'Hondt, A.J. Deruytter, Phys. Rev. C 23 (1981) 2104.
[76] H. Thierens, A. De Clercq, E. Jacobs, M. Piessens, P. D'Hondt, D. De Frenne, Phys. Rev. C 27 (1983) 1117.
[77] H. Thierens, E. Jacobs, P. D'Hondt, A. De Clercq, M. Pierssens, D. De Frenne, Phys. Rev. C 29 (1984) 498.
[78] T.D. Thiep, N.V. Do, N.K. Thi, T. Thi, N.G. Son, Comm. Phys. 14 (2004) 42.
[79] J.B. Laidler, F. Brown, J. Inorg. Nucl. Chem. 24 (1962) 1485.
[80] W.R. Nelson, H. Hirayama, D.W.O. Rogers, MAC report 265, 1985.
[81] A.I. Blokhin, A.S. Soldatov, Phys. At. Nucl. 72 (2009) 917.
[82] J.T. Caldwell, E.J. Dowdy, B.L. Berman, R.A. Alvarez, P. Meyer, Phys. Rev. C 21 (1980) 1215.
[83] M. Veyssiere, H. Bell, R. Bergere, P. Carlos, A. Lepretre, K. Kernbath, Nucl. Phys. A 199 (1973) 45.
[84] A.S. Soldatov, A.I. Blokhin, A.V. Ignatyuk, A.N. Storozhenko, Phys. At. Nucl. 63 (2000) 31.
[85] A.J. Koning, S. Hilaire, M.C. Duijvestijn, in: Proceedings of the International Conference on Nuclear Data for Science and Technology, ND 2004, vol. 769, Sept. 26–Oct. 1 (2004) Santa Fe, USA, AIP, 2005, p. 1154.
[86] H. Naik, S. Singh, A.V.R. Reddy, V.K. Manchanda, S. Ganesan, D. Raj, Md. Shakilur Rahman, K.S. Kim, M.W. Lee, G. Kim, Y.D. Oh, H.-S. Lee, M.-H. Cho, I.S. Ko, W. Namkung, Eur. Phys. J. A 41 (2009) 323.
[87] E. Browne, R.B. Firestone, in: V.S. Shirley (Ed.), Table of Radioactive Isotopes, 1986;
R.B. Firestone, L.P. Ekstrom, WWW Table of Radioactive Isotopes, Ver. 2.1, available at http://ie.lbl.gov.toi/.
[88] J. Blachot, Ch. Fiche, Table of radioactive isotopes and their main decay characteristics, Ann. Phys. 6 (1981) 3–218.
[89] K. Persyn, E. Jacobs, S. Pomme, D. De Frenne, K. Govaert, M.-L. Yoneama, Nucl. Phys. A 620 (1997) 171.
[90] S. Pomme, E. Jacobs, K. Persyn, D. De Frenne, K. Govaert, M.L. Yoneama, Nucl. Phys. A 560 (1993) 689.
[91] H. Naik, R.J. Singh, R.H. Iyer, Eur. Phys. J. A 16 (2003) 495.
[92] N. Sugarman, A. Turkevich, in: C.D. Coryell, N. Sugarman (Eds.), Radiochemical Studies: The Fission Product, McGraw-Hill, New York, 1951, p. 1396.
[93] H.N. Erten, N.K. Aras, J. Inorg. Nucl. Chem. 41 (1979) 149.
[94] C.D. Coryell, M. Kaplon, R.D. Fink, Can. J. Chem. 39 (1961) 646.
[95] P. Moller, Nucl. Phys. A 192 (1972) 529.
[96] M.L. Yoneama, E. Jacobs, J.D.T. Arruda-Neto, B.S. Bhandari, D. De Frenne, S. Pomme, K. Persyn, K. Govaert, Nucl. Phys. A 604 (1996) 263.
[97] H. Naik, S.P. Dange, A.V.R. Reddy, Nucl. Phys. A 781 (2007) 1.
[98] U. Brossa, S. Grossmann, A. Muller, Phys. Rep. 197 (1990) 167.
[99] B.D. Wilkins, E.P. Steinberg, R.R. Chasman, Phys. Rev. C 14 (1976) 1832.